Enormous spin polarization in heavy-ion-induced one-nucleon transfer reactions

Yuichi Yamamoto and Ken-Ichi Kubo
Department of Physics, Tokyo Metropolitan University, 1-1 Minami-ohsawa, Hachiohji, Tokyo 192-03, Japan
(Received 26 July 1993)

We show a possible large spin polarization of nuclei produced by one-nucleon transfer reactions predicted by the direct reaction theory. We investigate its origins in terms of the magnetic-sub-state cross sections by decomposing those into near-side and far-side components. The asymmetry of the particle-γ angular correlation followed by decay of the spin-polarized nucleus is also calculated.

PACS number(s): 24.70.+s, 24.50.+g, 25.70.Hi

I. INTRODUCTION

Studies of the spin polarization of reaction products are less common compared with the analyzing power measurements. One reason for this is the technical complications of polarization measurement, and the other is the existence of the polarization-asymmetry theorem. However, the theorem does not apply to the case of spin polarization of particles from non-ground-state nucleon-transfer interactions. Measurements of the spin polarization in such cases are carried out by measuring the asymmetric angular distribution of the correlated ejectile and decay particle, such as α, β, γ, and nucleons. The measurements are, therefore, quite difficult but challenging and are sometimes considered exotic experiments.

These are the reasons, whether or not the magnitude of the polarization becomes large or small, why the dynamics is so much less well studied in both experiment and theory. Another reason to call such experiments exotic is perhaps to stress the idea of using such polarized unstable nuclei as the injectile (secondary) beams for the new reaction experiments, which cannot be studied using the stable nuclei as the projectile and targets. Therefore, it would be extremely interesting and important if we could find some case where the spin of the reaction products is highly polarized and also know the dynamics providing it.

In this paper we show some unique cases where a large spin polarization of the reaction products may occur. We also explain what the results of large spin polarization are.

In the following, we first briefly review the past studies of the spin polarization of unstable nuclei in both the experimental and theoretical works. Spin polarization of ^{12}B produced through the reaction ^{11}B$(d,p)^{12}$B was measured by Berlijin *et al.*, and Pfeiffer and Madansky in 1967 [1] using coincidence measurements of the proton and decaying β ray, and it is found to be about 5% for the deuteron energies 0.8–3.2 MeV. In 1977 the same ^{12}B polarization was measured by Sugimoto *et al.* [2] through the heavy-ion reaction ^{100}Mo(^{14}N, ^{12}B)^{102}Ru at 90-MeV incident energy. The polarization is about 30% in the small Q-value region, and it rapidly decreases with the increase of the Q value by changing the sign from positive to negative. This result attracted theoretical attention, and several models interpreting the result were proposed [3,4]. In Ref. [3] Ishihara *et al.* reported that the frictional force alone was not able to account for the whole feature of the Q-value dependence, but the semiclassical description proposed by Brink [5], together with consideration of the continuum final states, qualitatively explains the observed sign and magnitude of polarization only in the quasielastic region. As a more quantitative treatment of this reaction, the exact finite-range (EFR) distorted wave Born approximation (DWBA) calculation that properly includes the continuum final states has been performed by Udagawa and Tamura and gives an almost complete interpretation of the quasielastic region [4]. Three other experiments calculating the ^{12}B polarization have been made in 1978–79 on the reactions [6] ^{100}Mo(^{14}N, ^{12}B)^{102}Ru at 200 MeV, ^{197}Au(^{19}F, ^{12}B)^{204}Bi at 186 MeV, and ^{232}Th(^{13}C, ^{12}B)^{233} Pa at 149 MeV.

Recently the (^{14}N, ^{12}B) reaction on ^{197}Au at the 560-MeV incident energy was carried out by Asahi *et al.*, and polarization changing from +20 to −10% as the Q value increases was observed [7]. The simple semiclassical [7] and semiquantal microscopic [8] calculations have been made and both give a successful interpretation of the results. In Ref. [8] Ohnishi, Maruyama, and Horiuchi show that the origin of the ejectile polarization can be understood clearly by studying separately the near-side and far-side contributions to the polarization.

In deep inelastic collisions, small (+25%) and large (+80%) polarizations of the excited nuclei were reported by Lauterbach *et al.* [9] and by Trautmann *et al.* [10] for the collisions using different sets of nuclei and energies; the polarization was deduced by measuring the circular polarization of the deexcitation γ ray. The presence of negative scattering angles (far-side trajectories) on the basis of the frictional picture was found to be consistent with the observed results [10].

In 1979 the spin polarizations of the excited 3^-, 5^-, and 6^+ states of ^{20}Ne were measured by Pougheon *et al.* [11] using the ^{12}C-α angular correlation measurement of the ^{16}O(^{16}O, ^{12}C)^{20}Ne reaction. The magnitude changes from 70 to 90% as the ^{12}C scattering angle changes from 10° to 40°. The polarization in this case corresponds to that of the orbital angular momentum transferred to the residual nucleus. The EFR-DWBA calculation reproduces the observed angular shape, but its magnitude is

smaller by a factor of about 1.3 compared with the observed results. The authors pointed out that a simple friction model is not inconsistent with the observed polarization if such an extreme condition for the trajectory is accepted that only one (near- or far-) side trajectory is effective for the transfer reaction. However, the friction model is, in general, too simple to predict the polarization of the residual nuclei excited in the discrete levels. This conclusion is the same as Bond pointed out in Ref. [12]. He also studied the heavy-ion polarization and Q-value dependence of its sign using a semiclassical expression derived from the no-recoil DWBA amplitude [13].

The polarization produced by the spin-orbit distortion has been estimated by Ellis [14] in the framework of the no-recoil DWBA calculation for the $^{14}N(1^+)$ as 30% in the one-nucleon transfer $^{40}Ca(^{13}C,^{14}N)^{39}K$ and for the $^{31}P(1/2^+)$ as 70% in the three-nucleon transfer $^{28}Si(^{19}F,^{16}O)^{31}P^*$ reactions, but no experimental measurement has been reported yet.

In this paper, we describe some unique cases producing a large spin polarization of the final nuclei produced by the simple one-nucleon-transfer reactions to the discrete final states. We predict those results by the exact-finite-range DWBA calculations. A brief result has been reported in Ref. [15]. We investigate the dynamics producing such a large polarization using the semiclassical description based on the Brink's matching condition [5]. We will emphasize in our semiclassical treatment that the Brink's condition should be carefully applied when we discuss the matching conditions of the near- and far-side cross sections. One of Brink's conditions (for angular-momentum matching) is equivalent to the picture used by Asahi *et al.* [7] in his interpretation of the polarization in the fragmentation reactions, and it is also closely related to the semiclassical treatment based on the no-recoil DWBA given by Bond [13]. However, as was shown in our previous paper [15], it is indispensable for some reactions considered here to treat the recoil effect properly, and in this case Brink's other condition (for the linear momentum matching) will be shown to play an important role.

In Sec. II, we show our calculated polarization. The dynamics producing such a polarization are investigated in Sec. III, where near-side and far-side contributions are treated separately and discussed using Brink's matching conditions, and in Sec. IV the total (near and far) polarization is discussed in connection with the relative importance between the near-side and far-side contributions. We will give the asymmetry of the particle-γ angular correlations emitted from the polarized nuclei in Sec. V. Conclusions are presented in Sec. VI.

II. THE RESULTS OF THE PRESENT CALCULATIONS

First we show the results of the exact finite-range DWBA calculation for several reactions in which a large spin polarization of the final nuclei occurs. In Fig. 1(a) we show our predictions for the case of two $p_{1/2}\rightarrow p_{1/2}$ transfer reactions: $^{12}C(^{13}C,^{12}C)^{13}C(g.s.,1/2^-)$ at $E_{lab}=140$ MeV and $^{54}Fe(^{13}C,^{12}C)^{55}Fe^*(0.41\ MeV,1/2^-)$ at $E_{lab}=60$ MeV. The spin polarizations of the residual nuclei among the $\mathbf{k}_a\times\mathbf{k}_b$ direction are presented, where $\mathbf{k}_a$ ($\mathbf{k}_b$) is momentum vector of the projectile (ejectile), respectively. We can see from Fig. 1(a) that (1) the magnitudes of the spin polarization are quite large in the two reactions, (2) their signs are almost independent on the scattering angles, and (3) they are completely reversed for the same $1/2^-$ residual states. We have chosen these two reactions and incident energies in order to demonstrate the dependence of the sign of polarization on the relative balance between the incident energy and the Coulomb barrier. We will study this later in detail.

Before we explain the dynamics providing these results, we present some cases. In Fig. 1(b), the $p_{3/2}\rightarrow p_{1/2}$ transition in the $^{12}C(^{12}C,^{13}C)^{11}C$ reaction at $E_{lab}=140$ and 300 MeV is shown, where a large polarization of the ejectile ^{13}C is predicted. We have also calculated spin polarizations induced by various one-nucleon-transfer reactions and found that in many cases final nuclei are to be polarized largely.

The exact finite-range DWBA calculations were performed using the computer code SATURN–MARS [16]. The distorting potentials reported in Refs. [17] and [18]

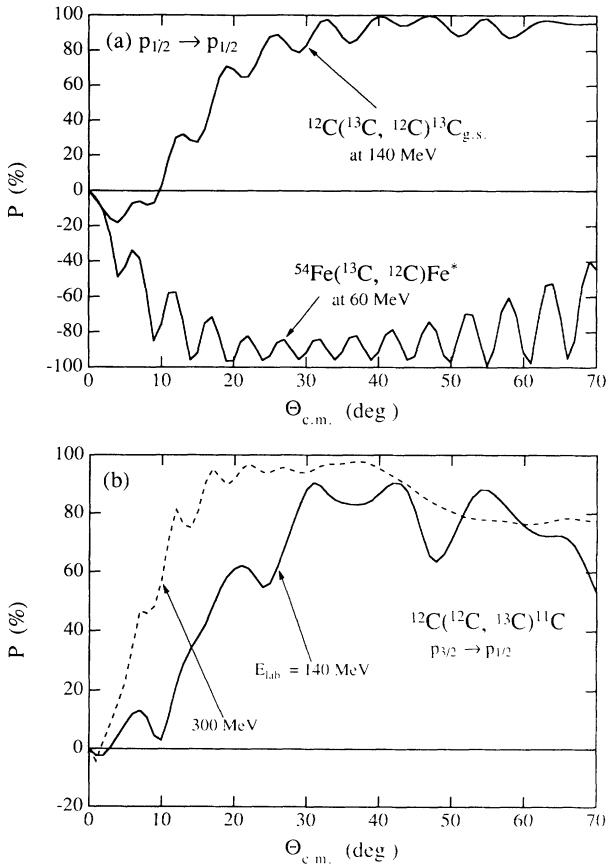

FIG. 1. Calculated spin polarizations of the final nucleus produced by the one-nucleon transfer reactions. (a) Spin polarizations of the residual nuclei produced by the two $p_{1/2}\rightarrow p_{1/2}$ transfer reactions, $^{12}C(^{13}C,^{12}C)^{13}C_{g.s.}$ at $E_{lab}=140$ MeV and $^{54}Fe(^{13}C,^{12}C)^{55}Fe^*(1/2^-)$ at $E_{lab}=60$ MeV, are compared. (b) Spin polarizations of the ejectile produced by the $p_{3/2}\rightarrow p_{1/2}$ transfer reaction $^{12}C(^{12}C,^{13}C)^{11}C$ at $E_{lab}=140$ and 300 MeV are shown.

were used for the $^{12}C(^{13}C,^{12}C)^{13}C$ and $^{12}C(^{12}C,^{13}C)^{11}C$ reactions at 140 MeV and for the $^{54}Fe(^{13}C,^{12}C)^{55}Fe^*$ reaction at 60 MeV, respectively. For the $^{12}C(^{12}C,^{13}C)^{11}C$ reactions at 300 MeV, the potential set labeled 25A in Ref. [19] were used. The distorted waves for the initial and final channels were generated using the same distorting potentials. The neutron-binding potentials are the Woods-Saxon form with $r_0=1.25$ fm, $a=0.65$ fm, and a spin-orbit term of strength $V_{\text{s.o.}}=8$ MeV. The strength of potential was determined to reproduce each experimental separation energy. The potential obtained is used as the transition interaction. The spectroscopic factors for the carbon nucleus were taken from Cohen and Kurath [20]; $S=0.6132$ for the $1p_{1/2}$ state in ^{13}C and $S=5.6989$ for the $1p_{3/2}$ state in ^{12}C. For the $2p_{1/2}$ state in ^{55}Fe we used $S=0.59$, which is deduced from the (d,p) reaction in Ref. [21]. The elastic-transfer-mechanism contribution to the $^{12}C(^{13}C,^{12}C)^{13}C$ reaction is not included in the calculation because we are interested in the spin polarization arising from the nucleon-transfer mechanism, and anyway the elastic transfer effect is small for the forward scattering angles [22].

In the following sections, we show that the origins of the large polarization and its sign can be understood by considering two aspects. In Sec. III we show the first one, that is, a strong selectivity of the semiclassical path through which the nucleon is transferred from the initial bound state to the final one. In Sec. IV we will discuss the second aspect, the preference of one of the classical trajectories, near or far side.

III. THE CROSS SECTIONS OF MAGNETIC SUB-STATE POPULATION AND THEIR NEAR-SIDE AND FAR-SIDE COMPONENTS

In order to investigate the dynamics of such a large spin polarization, it is very useful to express the spin polarization in terms of the magnetic sub-state population cross sections. Indeed, decomposing those population cross sections into the near-side and far-side components, we can understand the mechanisms producing a large polarization by using a semiclassical picture based on Brink's matching condition [5]. In the following, we first explain briefly the calculation methods needed for the analyses in Sec. III A and then interpret the calculated results in terms of Brink's matching condition in Sec. III B.

A. Calculation methods

1. *Decomposition of the DWBA amplitude into the near-side and far-side components*

The reduced transition amplitude β is defined as usual for the non-spin-orbit distortion case [23],

$$T_{M_B M_b M_A M_a}=\sum_{lsj}(2j+1)^{1/2} \times A_{lsj}(I_A M_A j\mu|I_B M_B)\beta_{sj}^{lmM_bM_a} , \quad (1)$$

where l and j are, respectively, the orbital and the total angular-momentum transfers, and m and μ are their z component. s is the spin transfer. I_A (M_A) and I_B (M_B) are, respectively, the spins (their z components) of target and residual nuclei, and M_a and M_b are the z component of spins of projectile (I_a) and ejectile (I_b), respectively. When we define the z axis to be parallel to the $\mathbf{k}_a$ and the y axial to $\mathbf{k}_a\times\mathbf{k}_b$, where $\mathbf{k}_a$ ($\mathbf{k}_b$) are, respectively, the momentum vector of the projectile (ejectile), the reduced amplitude may be represented in the form

$$\beta_{sj}^{lmM_BM_a}=\sum_{L_bL_a} a_{sj,L_bL_a}^{lmM_bM_a}P_{L_b}^{M_b}(\cos\theta) , \quad (2)$$

where $P_{L_b}^{M_b}$ are the associated Legendre functions and L_a and L_b are, respectively, partial waves for the initial and final channels, and $a_{sj,L_bL_a}^{lmM_bM_a}$ contain the geometrical factors and the overlap integrals. The decomposition of the amplitude into near-side (N) and far-side (F) components given by Fuller [24] is founded on writing $P_{L_b}^{M_b}$ as a sum of two terms,

$$P_{L_b}^{M_b}(\cos\theta)=Q_{L_b}^{M_b(-)}(\cos\theta)+Q_{L_b}^{M_b(+)}(\cos\theta) . \quad (3)$$

Here, the $Q_{L_b}^{M_b(\pm)}$ are defined by

$$Q_{L_b}^{M_b(\pm)}(\cos\theta)=\frac{1}{2}\left[P_{L_b}^{M_b}(\cos\theta)\mp\frac{2i}{\pi}Q_{L_b}^{M_b}(\cos\theta)\right] , \quad (4)$$

where $Q_{L_b}^{M_b}$ are the associated Legendre functions of the second kind. Then, near-side and far-side amplitudes are, respectively, given by

$$\beta_{sj}^{lmM_bM_a}(N,F)=\sum_{L_bL_a} a_{sj,L_bL_a}^{lmM_bM_a}Q_{L_b}^{M_b(\pm)}(\cos\theta) . \quad (5)$$

2. *The coordinate axes and spin-selection rules*

The near-far decomposition presented in the last section is defined in the coordinate system in which the z axis is defined along the direction of $\mathbf{k}_a$ and the y axis along $\mathbf{k}_a\times\mathbf{k}_b$. However, we are now discussing the spin polarizations and also the m sub-state populations with respect to the direction of the normal to the reaction plane. Therefore, it is convenient to rotate the coordinate system to the one in which the z axis is taken to be parallel to $\mathbf{k}_a\times\mathbf{k}_b$ and the x and y axes lie in the reaction plane (we take the x axis to lie along $\mathbf{k}_a$). Using rotation matrices [25], $\mathcal{D}$, we transform the reduced amplitudes into the new coordinate system,

$$\beta_{sj}^{lmM_bM_a}(\text{new})=\sum_{\mu'M_b'M_a'}\beta_{sj}^{lm'M_b'M_a'}(\text{old}) \times\mathcal{D}_{\mu\mu'}^{(j)*}\mathcal{D}_{M_b'M_b}^{(I_b)^*}\mathcal{D}_{M_a'M_a}^{(I_a)} , \quad (6)$$

where $\mu=m+M_a-M_b$ and $\mu'=m'+M_a'-M_b'$.

In the two coordinate systems, the same relation,

$$m=M_B-M_A+M_b-M_a , \quad (7)$$

should be satisfied, since in the heavy-ion reactions con-

sidered here the spin-orbit distortions are not included. In the DWBA formalism, the relation

$$m = m_2 - m_1 \tag{8}$$

is implicitly included, where m_1 and m_2 are the z components of the orbital angular momenta of the bound nucleon before (l_1) and after (l_2) the transfer, respectively. In the new coordinate system it is known [23] that the additional selection rule,

$$m + l_1 + l_2 : \text{even} , \tag{9}$$

must be satisfied.

B. Brink's matching condition

In this section, we summarize the so-called Brink matching condition [5] for heavy-ion transfer reactions, with which we predict qualitatively the relative magnitudes among the m sub-state population cross sections as they will be shown in the next section. Usually the condition is used to predict the relative population probabilities among the final states with different spins, but we intend to apply the condition so as to predict the relative population probabilities among m sub-states with a certain spin. In Ref. [3] Ishihara *et al.* used the Brink condition for this purpose for the ^{100}Mo(^{14}N, ^{12}B)^{102}Ru reaction at 90 MeV to interpret the observed polarization of ejectile ^{12}B for the small-Q-value region. It should be noted that, in deriving the matching condition, the far-side dominance of the reaction was implicitly assumed by Brink [5]. The DWBA calculation done by Udagawa and Tamura [4] shows a possibility that the reaction considered in Ref. [3] is near-side dominant. Therefore, the work of Ref. [3] should be reinvestigated. In this work also we should be careful about this point, since as we will see later, we are discussing the near-side dominant reaction as well as the far-side dominant reaction. We apply a different matching condition for the near-side trajectories.

The Brink matching condition is extended into a general form including the case of a near-side trajectory. The condition consists of three kinematics.

(1) The matching condition for the linear momenta of the participating particles is as follows:

$$\Delta k = k_0 \pm \frac{m_1}{R_1} \pm \frac{m_2}{R_2} \approx 0 \tag{10}$$

(+ for the near-side and − for the far-side trajectory, respectively), where k_0 is the wave number of the projectile per nucleon in the laboratory system, and R_1 and R_2 are, respectively, the radii of projectile (target) and residual (outgoing) nucleus for the stripping (pickup) reaction. The restriction $|\Delta k| \approx 0$ is equivalent to the requirement that the x component (x axis$\|\mathbf{k}_a$) of the linear momenta of the transferred neutron should be almost conserved.

(2) The matching condition for the total angular momentum is

$$\Delta L = m_2 - m_1 \mp \{\tfrac{1}{2}k_0(R_1 - R_2) + Q(R_1 + R_2)/(\hbar v)\} \approx 0 , \tag{11}$$

where Q is the reaction Q value and v is the velocity of projectile in the laboratory system. The condition $|\Delta L| \approx 0$ is equivalent to the classical conservation low of the total angular momenta of the whole system; the first two terms in Eq. (11) represent the difference between angular momenta of the bound neutron in the initial and the final channel, and the third term is the change of the relative angular momentum of the two interacting nuclei. Further, the requirement that the transition probability is largest when the neutron is near the reaction plane leads us to the third condition.

$$(3)\ l_1 + m_1 : \text{even} , \quad l_2 + m_2 : \text{even} , \tag{12}$$

where l_1 and l_2 are the orbital angular momenta of the neutron in the initial and final bound states. These conditions have been shown to follow from the distorted-wave Born theory by Gross [26]. He has derived them by using the three-dimensional time-dependent JWKB approximation for distorted waves.

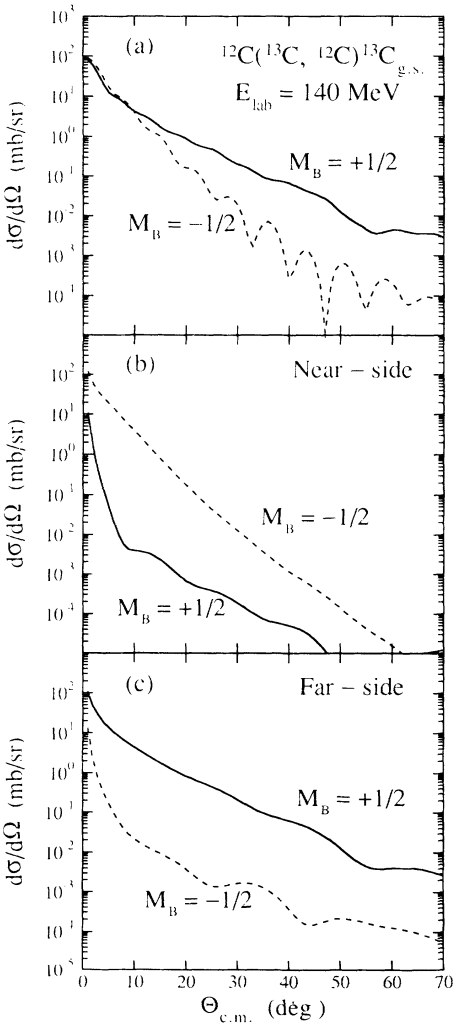

FIG. 2. The cross sections of the magnetic sub-state population for the spin states of the residual nucleus ^{13}C in the ^{12}C(^{13}C, ^{12}C)^{13}C$_{g.s.}$ reaction at E_{lab} = 140 MeV are shown in (a), and their near-side and far-side components are shown in (b) and (c), respectively.

C. The calculated m sub-state cross sections and applications of Brink's matching conditions

1. $p_{1/2} \rightarrow p_{1/2}$ transition

In Fig. 2, we show the calculated m sub-state population cross sections for the spin state of the residual nucleus ^{13}C for the $^{12}C(^{13}C,^{12}C)^{13}C(g.s.,1/2^-)$ reaction at $E_{lab}=140$ in Fig. 2(a). Their decompositions into the near-side and far-side components are shown in Figs. 2(b) and 2(c). The results of the $^{54}Fe(^{13}C,^{12}C)^{55}Fe^*(1/2^-)$ reaction at $E_{lab}=60$ MeV are shown in Fig. 3. We can see from Figs. 2(a) and 3(a) that, as expected from the polarizations shown in Fig. 1(a), the m sub-state cross sections $\sigma(M_B=+1/2)$ and $\sigma(M_B=-1/2)$ show large differences in magnitude. That is to say,

$$\sigma(M_B=+1/2)>\sigma(M_B=-1/2) \quad \text{for a } ^{12}C \text{ target} \tag{13a}$$

and, in contrast,

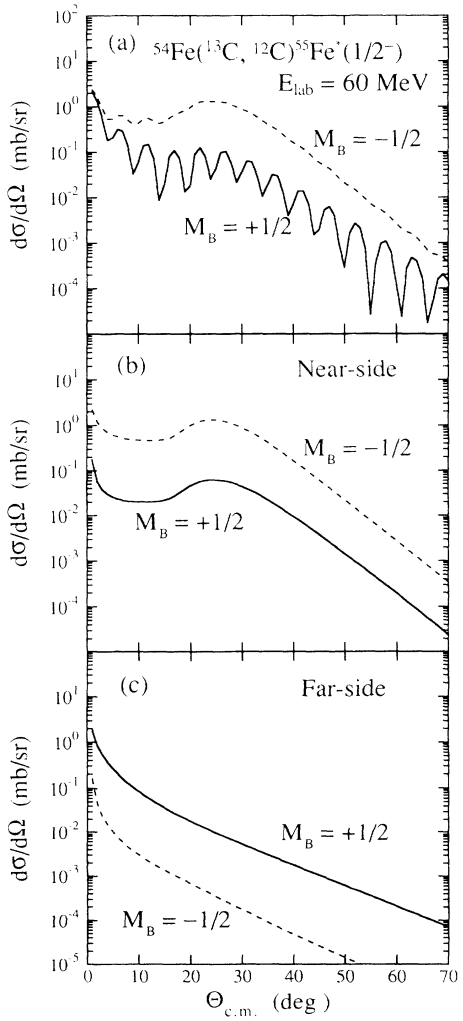

FIG. 3. The cross sections of magnetic sub-state population for the reaction $^{54}Fe(^{13}C,^{12}C)^{55}Fe^*(1/2^-; E_x=0.41$ MeV) reaction at $E_{lab}=60$ MeV are shown in (a), and their near-side and far-side components are shown in (b) and (c), respectively.

$$\sigma(M_B=+1/2)<\sigma(M_B=-1/2) \quad \text{for a } ^{54}Fe \text{ target} . \tag{13b}$$

These relations are almost independent on scattering angles, except for very forward angles. Figures 2(b), 2(c), 3(b), and 3(c) show one of the most remarkable features on the relative magnitudes of m sub-state cross sections. That is to say, as can be seen from Figs. 2(b) and 3(b), in the near side the cross section for $M_B=-1/2$ is about 1–3 orders of magnitude larger than that for $M_B=+1/2$ in the whole angular range. In contrast, Figs. 2(c) and 3(c) show that this relation in magnitudes of the cross sections for $M_B=\pm 1/2$ is completely reversed in the far-side trajectory. Then, we found the interesting feature, which is common in the two reactions, i.e.,

$$\sigma(M_B=+1/2)<\sigma(M_B=-1/2) \quad \text{for the near side} , \tag{14a}$$

$$\sigma(M_B=+1/2)>\sigma(M_B=-1/2) \quad \text{for the far side} . \tag{14b}$$

In the following, we show that dynamics producing these features can be interpreted by use of Brink's matching conditions mentioned in Sec. III B.

First we note that, since the spins I_A and I_b are both 0 in the reactions considered here, Eq. (7) can be written as

$$m=M_B-M_a . \tag{15}$$

Because l_1 and l_2 are both 1 and l takes 0 and 1, we get, from Eq. (9)

$$m=0 \tag{16}$$

for both $l=0$ and 1.

Now we interpret the possible combinations of m_1, m_2, M_a, and M_B with the semiclassical paths through which the nucleon is transferred and to which we apply Brink's matching conditions. Using Eqs. (8), (15), and (16), and considering condition (3) of Eq. (12), we get the two combinations in each near-side and far-side trajectory, which are shown in Table I. In this table, the z components of total angular momenta of the bound nucleon, m_{j_1} and m_{j_2}, are shown in the parentheses right after the corresponding z components of the orbital angular momenta. For the reactions considered here, $m_{j_1}=M_a$ and $m_{j_2}=M_B$. If we assume that the $p_{1/2}$ bound state can be described semiclassically as the state in which the intrinsic spin of the bound nucleon points in the opposite direction to its orbital angular momentum, we can associate these combinations with semiclassical paths depicted in Fig. 4 because the intrinsic spin of the transferred nucleon does not flip during transfer within our spin-independent interactions.

Then we evaluate $|\Delta k|$ and $|\Delta L|$ numerically. The values obtained are shown in the last four columns in Table I. We can see from the table that $|\Delta L|$'s are equal for all the paths in each reaction. On the other hand, $|\Delta k|$ for the path $N2$ is very small compared to that for

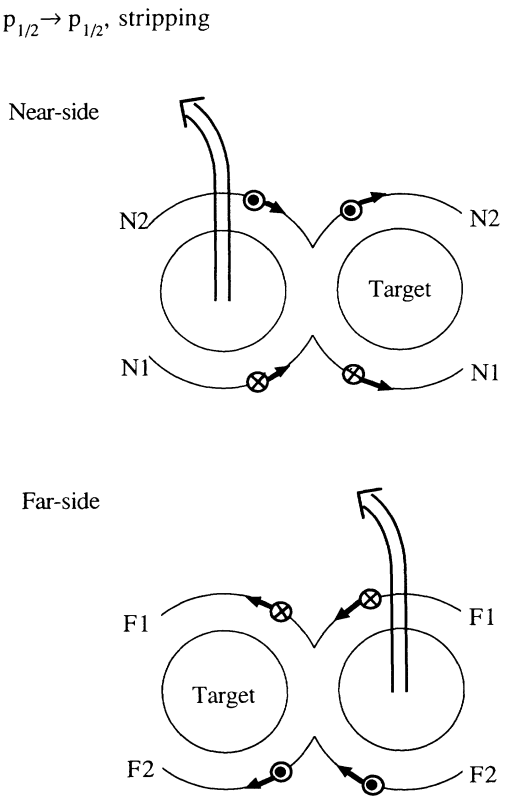

FIG. 4. The semiclassical paths through which one nucleon is transferred in the $p_{1/2} \rightarrow p_{1/2}$ stripping reaction. These paths correspond to the transitions given in Table I.

the path $N1$ in the near-side trajectory, which means that the transfer probability through the semiclassical path labeled $N2$ are to be much larger than that through $N1$ in the near-side trajectory. This is true for the two reactions. The transition, which corresponds to the semiclassical nucleon transfer through the path $N2$ leaves the residual nucleus ^{13}C in its spin state of $M_B = -1/2$. Consequently, the population for $M_B = -1/2$ dominates the near-side cross section. As to the far-side trajectory, since $|\Delta k|$ for $F1$ are much smaller than those for $F2$ in both reactions, the cross section for $M_B = +1/2$ becomes dominant. Now, we understand origin of the characteristic features shown in Figs. 2(b), 2(c), 3(b), and 3(c); the near-side cross section is dominated by the population $M_B = -1/2$ and the far side by the population $M_B = +1/2$.

As explained above, these results are caused from the matching condition for only the linear momentum of the transferred neutron. Therefore, this result is independent of the Q value. The effect arising from the Δk matching condition are called the TGV (Transfer à Grande Vitesse) effect by Von Oertzen [27]. With the effect, he has explained a spin selectivity and an exponential decrease of the cross section with respect to the incident energy in the range $E/A = 30$–90 MeV for the heavy-ion one-nucleon transfer reactions. Further, in terms of the DWBA amplitude, such a large difference in magnitude between m sub-state cross sections arises from the strong constructive or destructive interferences between amplitudes for angular momentum transfer $l = 0$ and 1 [15], that is, the amplitudes for the natural and unnatural parity transitions. In other words, within the no-recoil approximation the spin polarization does not occur in the $p_{1/2} \rightarrow p_{1/2}$ transfer. This situation is similar to that reported by Udagawa and Tamura in Ref. [4] for the $^{100}Mo(^{14}N, ^{12}B)^{102}Ru$ reaction at 90 MeV, where the exact-finite range DWBA calculation properly including the continuous final states have been performed. It is worthwhile to note that since the results shown above are caused by the kinematical reason, they can be a general feature for the $p_{1/2} \rightarrow p_{1/2}$ transfer reaction.

2. $p_{3/2} \rightarrow p_{1/2}$ transition

We show in Fig. 5(a) the calculated m-substrate cross sections for the spin-state of the ejectile ^{13}C of the $^{12}C(^{12}C, ^{13}C)^{11}C$ reaction at $E_{lab} = 140$ MeV and in Fig. 5(b) their near-side and in (c) their far-side components. As we can see in the figures, the differences in magnitudes between the cross sections for $M_b = \pm 1/2$ in each trajectory are again very large, and we found the relations

$$\sigma(M_b = +1/2) < \sigma(M_b = -1/2) \quad \text{for near side} , \tag{17a}$$

$$\sigma(M_b = +1/2) > \sigma(M_b = -1/2) \quad \text{for far side} . \tag{17b}$$

The dynamics producing the difference in magnitudes is also due to the kinematical matching condition as will be discussed below.

Since I_a and I_A are both 0 in this reaction, we can write Eq. (7) as

TABLE I. The possible combinations of z components of the projectile spin (I_a), the residual spin (I_B), and the orbital angular momentum (l_1 and l_2) for the transition $p_{1/2} \rightarrow p_{1/2}$. $N1$, etc., indicate the paths defined in Fig. 4. In the last four columns the values obtained by the Brink's matching conditions are shown.

Path	$m_1\ (m_{j_1}) \rightarrow m_2\ (m_{j_2})$	M_a	M_B	$^{12}C(^{13}C, ^{12}C)$ $\lvert\Delta k\rvert$	$\lvert\Delta L\rvert$	$^{54}Fe(^{13}C, ^{12}C)$ $\lvert\Delta k\rvert$	$\lvert\Delta L\rvert$
			Near side				
$N1$	$+1(+1/2) \rightarrow +1(+1/2)$	$+1/2$	$+1/2$	1.4	0.0	1.0	1.1
$N2$	$-1(-1/2) \rightarrow -1(-1/2)$	$-1/2$	$-1/2$	0.03	0.0	0.08	1.1
			Far side				
$F1$	$+1(+1/2) \rightarrow +1(+1/2)$	$+1/2$	$+1/2$	0.03	0.0	0.08	1.1
$F2$	$-1(-1/2) \rightarrow -1(-1/2)$	$-1/2$	$-1/2$	1.4	0.0	1.0	1.1

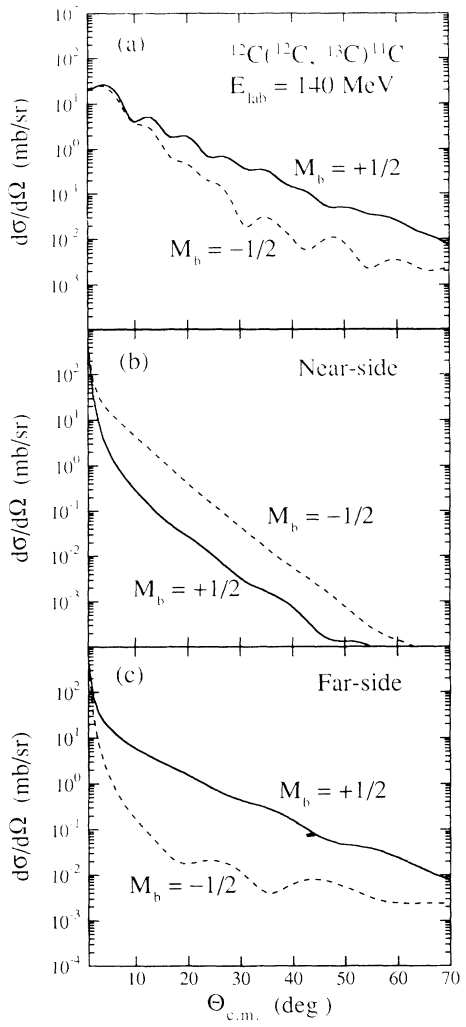

FIG. 5. The cross sections of magnetic sub-state population of the ejectile spin state in the $^{12}C(^{12}C,^{13}C)^{11}C$ reaction at $E_{lab}=140$ MeV are shown in (a), and their near-side and far-side components are shown in (b) and (c), respectively.

$$m = M_B + M_b \ . \tag{18}$$

From Eq. (9), we get

$$m = 0, \pm 2 \tag{19}$$

because l_1 and l_2 are equal to 1, and in the present transition l takes 1 and 2. Using Eqs. (8), (18), and (19), four possible combinations of m_1, m_2, M_b, and M_B are obtained in each trajectory, which are given in Table II. In this reaction, $m_{j_1} = -M_B$ and $m_{j_2} = M_b$. The populations of $M_b = +1/2$ are given by the sum of the contributions from $N1$ and $N2$ in the near side and from $F1$ and $F2$ in the far side, and the population of $M_b = -1/2$ is given by those from $N3$ and $N4$ in the near side and $F3$ and $F4$ in the far side. We associate these combinations with the semiclassical paths to which we apply the matching conditions, where we assume the $p_{3/2}$ states, with their z components m_{j_1} of the total angular momentum j_1 being $\pm 3/2$ ($\pm 1/2$), as states in which spin of the bound nucleon is parallel (antiparallel) to the orbital angular momentum l_1, which is depicted in Fig. 6.

We show, in Table II, the values of $|\Delta k|$ and $|\Delta L|$ for each path, and we show the cross sections corresponding to the $N1$–$N4$ in Fig. 7(a) and $F1$–$F4$ in Fig. 7(b). We can see from the values for the paths $N2$ and $N3$ in Table II that, while $|\Delta k|$'s are 0.7 for both, $|\Delta L|$ are 0.6 for $N3$ and 4.6 for $N2$; then, between these two paths, the transfer probability through the $N3$ is to be larger compared to that through the $N2$. We can also see that the transfer probability through the $N4$ should become larger than that through the $N1$ because of the relative magnitudes of $|\Delta k|$. ($|\Delta L|$'s for $N4$ and $N1$ are equal to each other.) Therefore, we can qualitatively understand the results shown in Fig. 7(a) that the cross sections labeled $N3$ (dotted curve) and $N4$ (dot-dashed curve) are much larger than those labeled $N1$ (solid curve) and $N2$ (dashed curve). Since $N3$ and $N4$ both leave the ejectile ^{13}C in the m sub-state $M_B = -1/2$, we get the results that the population $M_B = -1/2$ dominates the near-side cross section

TABLE II. The possible combinations of z components of the ejectile spin (I_b), the residual spin (I_B), and the orbital angular momentum (l_1 and l_2) for the transition $p_{3/2} \rightarrow p_{1/2}$. $N1$, etc., indicate the paths defined in Fig. 6. In the last four columns the values obtained by the Brink's matching conditions are shown.

Path	m	$m_1\ (m_{j_1}) \rightarrow m_2\ (m_{j_2})$	M_b	M_B	$\lvert\Delta k\rvert$	$\lvert\Delta L\rvert$
		Near side				
$N1$	0	$+1(+1/2) \rightarrow +1(+1/2)$	$+1/2$	$-1/2$	1.4	2.6
$N2$	$+2$	$-1(-3/2) \rightarrow +1(+1/2)$	$+1/2$	$+3/2$	0.7	4.6
$N3$	-2	$+1(+3/2) \rightarrow -1(-1/2)$	$-1/2$	$-3/2$	0.7	0.6
$N4$	0	$-1(-1/2) \rightarrow -1(-1/2)$	$-1/2$	$+1/2$	0.06	2.6
		Far side				
$F1$	0	$+1(+1/2) \rightarrow +1(+1/2)$	$+1/2$	$-1/2$	0.06	2.6
$F2$	$+2$	$-1(-3/2) \rightarrow +1(+1/2)$	$+1/2$	$+3/2$	0.7	0.6
$F3$	-2	$+1(+3/2) \rightarrow -1(-1/2)$	$-1/2$	$-3/2$	0.7	4.6
$F4$	0	$-1(-1/2) \rightarrow -1(-1/2)$	$-1/2$	$+1/2$	1.4	2.6

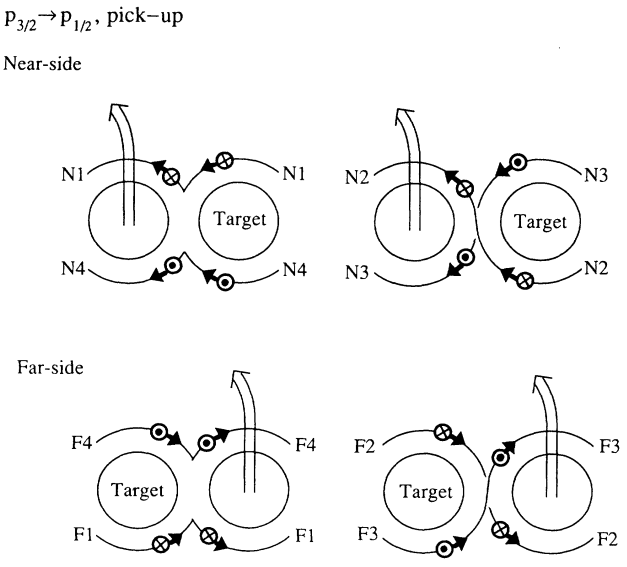

FIG. 6. The semiclassical paths through which one nucleon is transferred in the $p_{3/2} \rightarrow p_{1/2}$ pick-up reaction. These paths correspond to the transitions given in Table II.

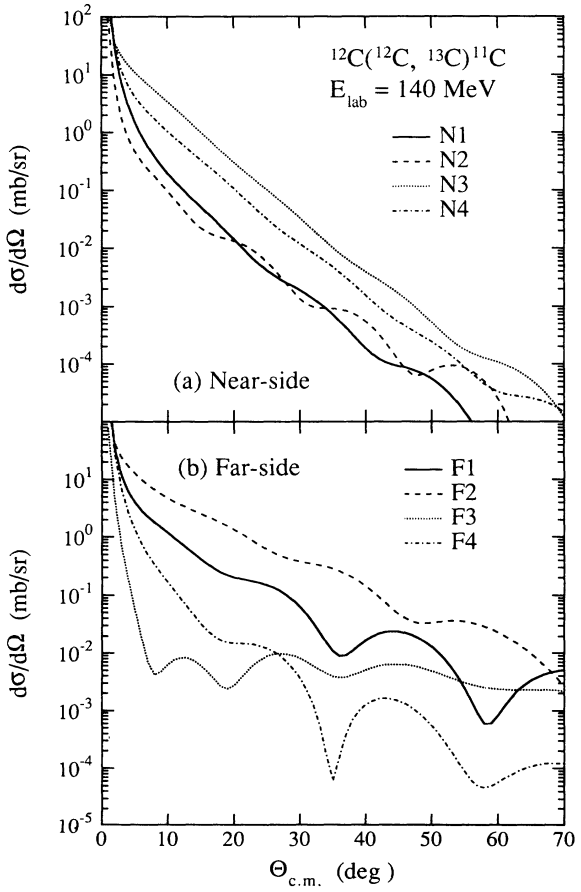

FIG. 7. The cross sections corresponding to the various paths in the near-side (a) and the far-side (b) trajectories. The meaning of the curves labeled $N1$–$N4$ and $F1$–$F4$ is shown in Table II and depicted schematically in Fig. 6.

[see Fig. 5(b)]. As to the far-side trajectory, we can expect that the cross section corresponding to $F2$ becomes much larger than that corresponding to $F3$ from the values of $|\Delta L|$, and $F1$ than $F4$ from the values of $|\Delta k|$. The paths $F1$ and $F2$ both leave ^{13}C in the $M_B = +1/2$ population, then this population dominates the far-side trajectory as shown in Fig. 5(c).

It is worthwhile noting that for the present $p_{3/2} \rightarrow p_{1/2}$ transition, in contrast to the $p_{1/2} \rightarrow p_{1/2}$ transition, the matching condition for the total angular momentum plays an important role as well as that for linear momentum of the transferred nucleon. Then, as is clear from the expression of Eq. (11), the sign and magnitude of the polarization is expected to depend on the reaction Q value. Indeed, we have found that DWBA calculations show those dependences. A similar result has been reported and discussed by using the semiclassical picture by Bond [13]. The work of Asahi *et al.* [7] and Ohnishi, Maruyama, and Horiuchi [8] discussing the sign of spin polarization of the fragmentation reaction $^{197}Au(^{14}N, ^{12}B)$ at $E_{lab} = 560$ MeV can be reinvestigated using the ΔL-matching condition (11). As explained above, the origin of the *large* difference in magnitude of the cross sections can be understood with the semiclassical concept. However, a difference between cross sections, where magnitudes are not so much different from each other, such as between $N3$ and $N4$, cannot be accounted for by the present semiclassical description. Indeed, the relative magnitudes among such cross sections show a rather strong dependence on the distorting potentials [28]. But we have confirmed that the largely different cross sections do not change by using the different sets of distorting potentials.

IV. SIGN OF THE POLARIZATION

A. The relative strength of the near-side and far-side amplitudes

In Sec. III we have discussed the m sub-state cross sections of each near-side and far-side trajectory. In this section we investigate the characteristics of the total (near and far) m sub-state cross sections. We discuss the sign of the total polarization in connection with the relative magnitude between the near-side and far-side cross sections.

First, we consider the $p_{1/2} \rightarrow p_{1/2}$ transition. We have shown in Sec. II that sign of the polarization of the residual nucleus is positive for the $^{12}C(^{13}C, ^{12}C)^{13}C$ reaction at 140 MeV, and it is negative for the $^{44}Fe(^{13}C, ^{12}C)^{55}Fe^*$ reaction at 60 MeV. These results of sign can be attributed to the fact that the far-side trajectory is dominant for the former case, and the near-side trajectory is dominant for the latter case. This is as we have discussed in Sec. II, due to, the fact that the cross section of the population $M_B = -1/2$ is dominant in the near-side trajectory and that of $M_B = +1/2$ is dominant in the far-side trajectory. Indeed, we can see from Fig. 2 for the ^{12}C-target case that although the m sub-state cross section for $M_B = +1/2$ in the far-side [solid curve in Fig. 2(c)] and that for $M_B = -1/2$ in the near-side [dashed curve in

Fig. 2(b)] equally satisfy the kinematical matching conditions better than the other m sub-state cross section in each trajectory, the former cross section is much larger than the latter one. The preference of the former cross section arises from the predominant nuclear attractive force for the ^{12}C-target case at energy much above the Coulomb barrier. Further, the magnitude of the cross section for $M_B=-1/2$ in the near-side trajectory is as small as that for $M_B=-1/2$ in the far-side trajectory; therefore, the total $M_B=-1/2$ population cross section shows strong oscillation due to the near-far interference. As to the ^{54}Fe-target case, at energy near the Coulomb barrier, this situation is reversed with a predominance of the $M_B=-1/2$ cross section in the near-side trajectory. Thereby the polarization sign becomes negative.

In order to demonstrate this incident energy dependence clearly, we show in Fig. 8 the calculated polarizations of ^{13}C in the ^{12}C(^{13}C, ^{12}C)^{13}C reaction at $E_{\rm lab}=140$, 60, and 20 MeV using the same distorting potential parameter set as that found at $E_{\rm lab}=140$ MeV. We can see that, as the incident energy decreases, sign of the polarization changes from positive to negative. This is because, while the near-side cross section becomes larger, the far-side cross section becomes smaller with the decreasing incident energy.

As is clear from the above considerations, one of the origins of large polarization is attributed to the large difference in magnitude between the near-side and far-side cross sections. Independence of the sign of the polarization on the scattering angles is caused by dominance of one trajectory on the wide angular range.

As to the $p_{3/2}\rightarrow p_{1/2}$ transition, i.e., ^{12}C(^{12}C, ^{13}C)^{11}C, at $E_{\rm lab}=140$ MeV, we have shown the results of polarization calculation in Fig. 1(b). Since, at this energy above the Coulomb barrier, the far-side contribution becomes dominant and the $M_b=+1/2$ cross section becomes dominant, as we have seen in Fig. 5, the sign of the total polarization becomes positive. We have also shown in Fig. 1(b) the polarization of the same reaction at $E_{\rm lab}=300$ MeV. At this higher energy, the far-side dominance begins at the more forward angles than is the case at $E_{\rm lab}=140$ MeV. Namely, at the forward angles the magnitude of the polarization at $E_{\rm lab}=300$ MeV is larger than that at 140 MeV.

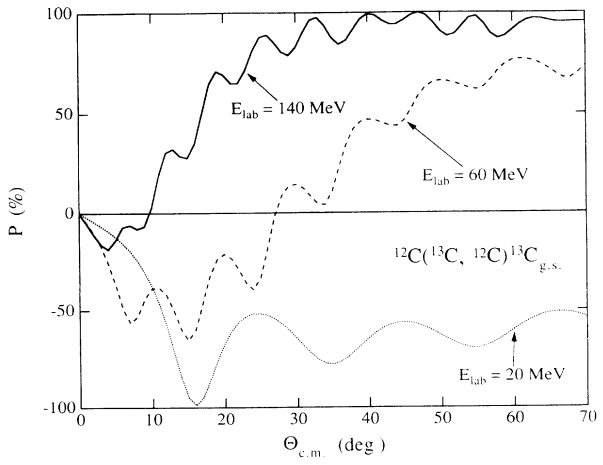

FIG. 8. The incident energy dependence of spin polarizations of the residual nucleus ^{13}C produced by the ^{12}C(^{12}C, ^{13}C)^{11}C reaction. The spin polarizations are calculated at $E_{\rm lab}=140$, 60, and 20 MeV using the same distorting potentials found at 140 MeV.

The relation between sign of the polarization and the relative near and far strength has been discussed by Bond [13]. The present more accurate calculation gives qualitatively similar results as his calculation, but the magnitude of the polarization is much higher in our prediction than in his results.

B. Predominance of one trajectory

In this section, we show how the relation between incident energy and relative magnitude of the amplitudes between near-side and far-side trajectories is determined in the framework of DWBA. In the general expression of the DWBA amplitude, the product of spherical harmonics appears:

$$Y_{L_a}^{M_a^*}(\theta_a,\phi_a)Y_{L_b}^{M_a-m}(\theta_b,\phi_b)\ , \tag{20}$$

where L_a and L_b are the partial angular momenta in the initial and final channels, respectively, M_a is the z component of L_a, and θ_i's and ϕ_i's ($i=a,b$) represent directions of linear momenta of the projectile $\mathbf{k}_a$ and ejectile $\mathbf{k}_b$. In most DWBA computer codes, the z axis is taken to be parallel to $\mathbf{k}_a$ and the y axis to $\mathbf{k}_a\times\mathbf{k}_b$, for convenience. For the present discussion, however, it is useful to choose the z axis parallel to the direction of $\mathbf{k}_a\times\mathbf{k}_b$ and the x axis along $\mathbf{k}_a$. In this coordinate system we get $\theta_a=\theta_b=\pi/2$, $\phi_a=0$, and $\phi_b=\theta_{\rm scatt}$, where $\theta_{\rm scatt}$ is the scattering angle. Therefore, we can write the $\theta_{\rm scatt}$-dependent part of expression (20) as

$$Y_{L_a}^{M_a^*}(\pi/2,0)Y_{L_b}^{M_a-m}(\pi/2,\theta_{\rm scatt})\rightarrow e^{i(M_a-m)\theta_{\rm scatt}}\ . \tag{21}$$

In this coordinate system, the near-side (far-side) amplitude corresponds semiclassically to that of the negative (positive) sum over M_a, respectively. This definition of near-side and far-side amplitudes gives almost the same results as that described in Sec. III A 1 according to Fuller's method. This correspondence is better for the higher partial waves, that is, for the strong absorptive heavy-ion reactions.

It is worthwhile to note that, as is known from the definitions, the near-side and the far-side amplitudes at a given partial wave differ from each other only by the phase factor, namely, the two amplitudes have the same absolute magnitudes. In other words, the large difference in magnitude between the near-side and the far-side amplitudes after taking the sum over the partial waves arises from the different interference natures among the partial amplitudes. That is to say, it is expected that the phase of partial amplitudes of the dominant trajectory should not be so different from each other, and then after taking the sum over the partial wave, a large amplitude is obtained. In contrast, for the other trajectory, the phases of partial amplitudes change largely from partial wave to partial wave. We show in the following that this feature

of the phases of partial amplitudes can be seen clearly in the DWBA amplitudes.

We consider the $^{12}C(^{13}C,^{12}C)^{13}C$ reaction. The partial-wave-dependent phases of the partial amplitudes arise from the two factors; the overlap integral and the spherical harmonics. The phases of spherical harmonics is $M_a\theta_{\rm scatt}$ ($m=0$ in the present case) and, in the following, we replace this phase by $-L_a\theta_{\rm scatt}$ for the near-side and $+L_a\theta_{\rm scatt}$ for the far-side trajectories by assuming the amplitudes corresponding to the $|M_a|=L_a$ may provide a large contribution. The phases of the partial overlap integrals come from those of the distorted waves for the initial and final channels. If we assume that the real part of the distorting potentials is preferential to their imaginary part, the distorted waves can be separated into the radial part and the phase such as,

$$\chi_{L_a}(r)=R_{L_a}(r)e^{i\sigma_{L_a}}, \tag{22}$$

where $R_{L_a}(r)$ is a real function and σ_L is the phase shift, which consists of nuclear and Coulomb parts. The phase of the overlap integral becomes $2\sigma_{L_a}$, because $L_b=L_a$ for the present reaction. Thus, we get the expression

$$T^{N/F}_{L_a}\propto e^{i(2\sigma_a\mp L_a\theta_{\rm scatt})}. \tag{23}$$

In order to show how these phases change with respect to L_a, we take the derivative of the phases with L_a. Using the well-known deflect-function relation

$$\theta_{\rm class}=\tfrac{1}{2}\frac{\partial\sigma_{L_a}}{\partial L_a}, \tag{24}$$

where $\theta_{\rm class}$ corresponds to the classical scattering angle associated with an L_a partial wave, we get the relation

$$\frac{\partial(2\sigma_{L_a}\mp L\theta_{\rm scatt})}{\partial L_a}=\theta_{\rm class}\mp\theta_{\rm scatt},$$

for near and/or far-side trajectories. (25)

Equation (25) says that for the near-side amplitudes the rate of the phase change with respect to the partial wave is given by the difference between the classical scattering angle associated with L_a and the scattering angle at which we detect the outgoing particle and, in contrast, for the far-side by sum of them. We depict in Fig. 9 the relations between those angles for the case of near-side scattering. We show in Figs. 9(a) and 9(b) the cases of the incident energies lower and higher than the Coulomb barrier, respectively. In these two figures the angle $\theta_{\rm scatt}$ is common at a certain positive value. For the lower incident energy case, $\theta_{\rm class}$ becomes positive due to the Coulomb repulsion, whereas for the higher incident energy case it becomes negative because of the strong nuclear attractive force. Therefore, $|\theta_{\rm class}-\theta_{\rm scatt}|$ in the former case becomes small compared to that in the latter case, namely, the amplitude of the former case after taking the sum over the partial waves becomes larger than that of the latter case. This is a consequence of difference in the interferences; the former case with the small

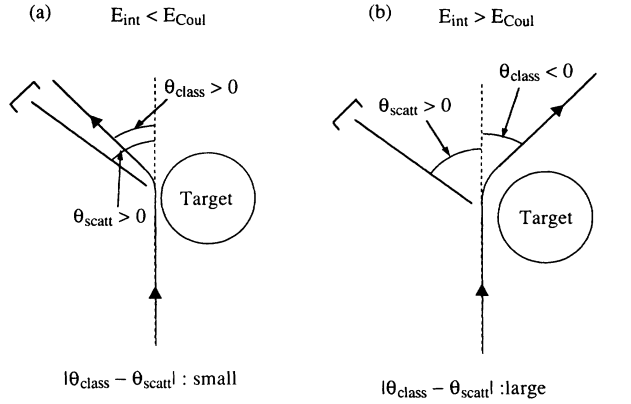

FIG. 9. The relations between angles $\theta_{\rm scatt}$ and $\theta_{\rm class}$ in the near-side scattering. Two cases of the incident energies, lower and higher than the Coulomb barrier, are shown in (a) and (b), respectively.

$|\theta_{\rm class}-\theta_{\rm scatt}|$ differences provides a constructive sum, whereas the latter case with the large difference does a destructive sum. In the far-side trajectory, the above relations are reversed due to a different sign appearing in Eq. (25), namely, the far-side amplitudes become larger as the incident energy increases.

V. ASYMMETRY OF γ RAY EMITTED FROM THE POLARIZED NUCLEI

The large spin polarization predicted in this paper for the $^{13}C_{\rm g.s.}$ in the $^{12}C(^{13}C,^{12}C)^{13}C$ and $^{12}C(^{12}C,^{13}C)^{11}C$ reactions can be detected by the double scattering experiment. On the other hand, for the case of the polarization of $^{55}Fe^*$ excited state in the $^{54}Fe(^{13}C,^{12}C)^{55}Fe^*(1/2^-)$ reaction, the particle-γ angular correlation technique may be used to observe the polarization. The angular distribution of the emitted γ ray (0.412 MeV) shows anisotropy if the spin of the intermediate state ($^{55}Fe^*$) is polarized. However, it is known that a γ ray decaying from the $\frac{1}{2}$-spin state shows an isotropic angular distribution unless the polarization of the emitted γ ray itself is observed [29]. In general, we can write the angular correlation function as [29]

$$W(\theta_\gamma)=W_L(\theta_\gamma)+W_R(\theta_\gamma), \tag{26}$$

where the first and second terms correspond to the left-hand and right-hand circularly polarized γ ray, respectively. Since we are considering the $M1$ transition of the $1/2^-$ state of $^{55}Fe^*$ to its ground state of $3/2^-$, they are given as

$$W_{L/R}(\theta_\gamma)=1\pm\tfrac{1}{2}P(\theta_{\rm c.m.})\cos\theta_\gamma, \tag{27}$$

where $\theta\gamma$ is the polar angle for the case of z axis defined as parallel to $\mathbf{k}_a\times\mathbf{k}_b$. $P(\theta_{\rm c.m.})$ is the polarization of $^{55}Fe^*$ as a function of the scattering angle ($\theta_{\rm c.m.}$) of outgoing ^{12}C. These functions are independent on the azimuthal angle and, as mentioned above, the sum of them, Eq. (20), are also independent on θ_γ. In Fig. 10, we show

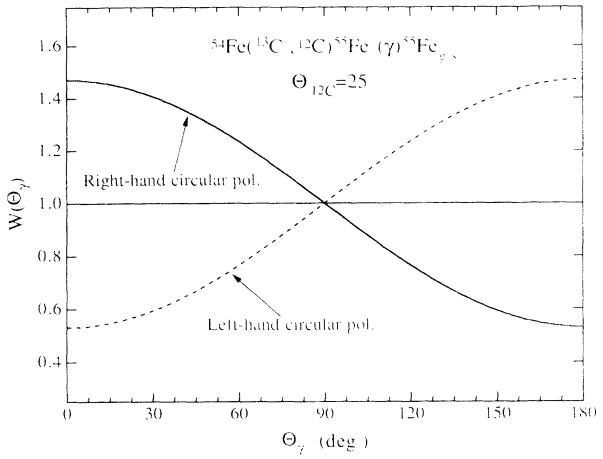

FIG. 10. The ^{12}C-γ angular correlation distributions for the ^{54}Fe(^{13}C,^{12}C)^{55}Fe* reaction at $\theta_{^{12}C}=25°$. The calculations are made for the γ rays of right-hand and left-hand circular polarizations emitted in the $M1$ transition from the 0.41 MeV $1/2^-$ excited state to the ground state of ^{55}Fe.

the calculated angular distributions of the angular correlation functions for the ^{12}C emission angle of $\theta_{c.m.}=25°$ ($P=-94\%$) for the ^{54}Fe(^{13}C,^{12}C)^{55}Fe*(γ)^{55}Fe$_{g.s.}$ reaction at $E_{lab}=60$ MeV. As shown in this figure, the asymmetry angular correlations between the ejectile and the γ ray emitted from the polarized nuclei show a maximum deviation of about 50% from the isotropic distribution.

It is extremely interesting and important to take measurements of polarizations by the double-scattering experiment or the angular correlation techniques to confirm the present predictions and to further extend spin physics using unstable polarized nuclei produced by the nuclear reactions.

VI. CONCLUSIONS

In this paper, we have shown that a possible large spin polarization of the nuclei produced by one-nucleon transfer reaction to the discrete final state may occur. We have shown the polarizations calculated by the EFR-DWBA for the four cases, that is, two $p_{1/2}\rightarrow p_{1/2}$ transfer reactions, ^{12}C(^{13}C,^{12}C)^{13}C at $E_{lab}=140$ MeV and ^{54}Fe(^{13}C,^{12}C)^{55}Fe*($1/2^-$) at $E_{lab}=60$ MeV, and the $p_{3/2}\rightarrow p_{1/2}$ transfer reaction ^{12}C(^{12}C,^{13}C)^{11}C at $E_{lab}=140$ and 300 MeV. Magnitudes of the polarizations reach almost 100% in these reactions at whole angular range, except for the very forward angles, and their signs are almost independent on the scattering angles.

Such a large polarization can be understood by considering the following facts. A strong selectivity of one or two paths out of the semiclassically possible nucleon transfer paths exist, through which a nucleon is transferred from the initial bound state to the final one. This selectivity arises from the kinematical matching conditions, which is described by the semiclassical picture based on Brink's matching condition. This kinematical matching condition becomes different between the near-side and the far-side trajectories, and, as a consequence, the sign of the polarization produced by the far-side predominance becomes opposite to that produced by the near-side predominance. This preference, which determines the sign of the total (near and far) polarization, is closely related to the relative magnitudes between the incident energy and the Coulomb barrier; therefore the sign of the polarization produced by a certain reaction shows the characteristic dependence on the incident energy.

As to the polarization of nucleus in the excited state such as ^{55}Fe*, we have shown that the asymmetry of angular correlation between the ejectile and γ ray emitted from the polarized nucleus can be used to observe the polarization. Other polarizations predicted in the present paper may be observed by using the double-scattering techniques.

It is extremely interesting and important to take these measurements of the polarization. Once these predictions are confirmed, we can further extend the nuclear spin physics using the largely polarized unstable nuclei as well as the stable nuclei produced by the nuclear reactions.

[1] J. J. Berlijn, P. W. Keaton, L. Madansky, G. E. Owen, L. Pfeiffer, and N. R. Roberson, Phys. Rev. **153**, 1152 (1967); Loren Pfeiffer and L. Madansky, *ibid.* **163**, 999 (1967).
[2] K. Sugimoto, N. Takahashi, A. Mizobuchi, Y. Nojiri, T. Minamisono, M. Ishihara, K. Tanaka, and H. Kamitsubo, Phys. Rev. Lett. **39**, 323 (1977).
[3] M. Ishihara, K. Tanaka, T. Kammuri, K. Matsuoka, and M. Sano, Phys. Lett. **73B**, 281 (1978).
[4] T. Udagawa and T. Tamura, Phys. Rev. Lett. **41**, 1770 (1978).
[5] D. M. Brink, Phys. Lett. **40B**, 37 (1972).
[6] N. Takahashi, Y. Miake, Y. Nojiri, T. Minanisono, A. Mizobuchi, M. Ishihara, and K. Sugimoto, Phys. Lett. **78B**, 397 (1978); M. Ishihara, T. Shimoda, H. Fröhlich, H. Kamitsubo, K. Nagatani, T. Udagawa, and T. Tamura, Phys. Rev. Lett. **43**, 111 (1979); M. Ishihara, in *Proceedings of the Symposium on the Continuum Spectra in Heavy Ion Collisions, San Antonio, 1979,* edited by T. Tamura, J. B. Natowitz, and D. H. Youngblood (Harwood Academic, Chur, Switzerland, 1979), p. 89.
[7] K. Asahi, M. Ishihara, N. Inabe, T. Ichihara, T. Kubo, M. Adachi, H. Takanashi, M. Kouguchi, M. Fukuda, D. Mikolas, D. J. Morrissey, D. Beaumel, T. Shimoda, H. Miyatake, and N. Takahashi, Phys. Lett. B **251**, 488 (1990).
[8] A. Ohnishi, T. Maruyama, and H. Horiuchi, Prog. Theor. Phys. **87**, 417 (1992).
[9] C. Lauterbach, W. Dünnweber, G. Graw, W. Hering, H. Puchta, and W. Trautmann, Phys. Rev. Lett. **41**, 1774 (1978).
[10] W. Trautmann, J. de Boer, W. Dünnweber, G. Graw, R. Kopp, C. Lauterbach, H. Puchta, and U. Lynen, Phys. Rev. Lett. **39**, 1062 (1977).
[11] F. Pougheon, P. Roussel, M. Bernas, F. Diaf, B. Fabbro, F. Naulin, E. Plagnol, and G. Rotbard, Nucl. Phys. **A325**, 481 (1979).
[12] P. D. Bond, Phys. Rev. Lett. **40**, 501 (1978).
[13] P. D. Bond, Phys. Rev. C **22**, 1539 (1980).
[14] P. J. Ellis, Nucl. Phys. **A302**, 257 (1978).

[15] Y. Yamamoto and K.-I. Kubo, Phys. Rev. Lett. **68**, 2588 (1992).
[16] T. Tamura and K. S. Low, Comput. Phys. Commun. **8**, 349 (1974).
[17] María-Ester Brandan, Phys. Rev. Lett. **60**, 784 (1988).
[18] F. D. Becchetti, P. R. Christensen, V. I. Manko, and R. J. Nickles, Nucl. Phys. **A203**, 1 (1973).
[19] G. R. Satchler, Nucl. Phys. **A505**, 103 (1989).
[20] S. Cohen and D. Kurath, Nucl. Phys. **A101**, 1 (1967).
[21] D. C. Kocher and W. Haeberli, Nucl. Phys. **A196**, 225 (1972).
[22] W. von Oertzen, in Proceedings of the INS-IPCR Symposium on Cluster Structure of Nuclei and Transfer Reactions Induced by Heavy-Ions, Tokyo, 1975, edited by H. Kamitsubo, I. Kohno, and T. Marumori (unpublished) p. 381.
[23] G. R. Satchler, Nucl. Phys. **55**, 1 (1964).
[24] R. C. Fuller, Phys. Rev. C **12**, 1561 (1975).
[25] D. M. Brink and G. R. Satchler, *Angular Momentum* (Oxford University Press, New York, 1962).
[26] D. H. E. Gross, Phys. Lett. **43B**, 371 (1973).
[27] W. Von Oertzen, Phys. Lett. **151B**, 95 (1985).
[28] Yuichi Yamamoto and Ken-Ichi Kubo (unpublished).
[29] H. J. Rose and D. M. Brink, Rev. Mod. Phys. **39**, 306 (1967); F. Rybicki, T. Tamura, and G. R. Satchler, Nucl. Phys. **A146**, 659 (1970).